Journal of Power Sources 202 (2012) 134–142

Contents lists available at SciVerse ScienceDirect

Journal of Power Sources

journal homepage: www.elsevier.com/locate/jpowsour

# Development of a 4-cell air-breathing micro direct methanol fuel cell stack

Zhenyu Yuan [a], Yufeng Zhang [a,b,*], Jiaxing Leng [a], Yuhan Gao [a], Xiaowei Liu [a,b]

[a] MEMS Center, Harbin Institute of Technology, Harbin 150001, China
[b] Key Laboratory of Micro-Systems and Micro-structures Manufacturing, Ministry of Education, Harbin 150001, China

ARTICLE INFO

*Article history:*
Received 19 September 2011
Received in revised form 22 October 2011
Accepted 24 October 2011
Available online 15 November 2011

*Keywords:*
Micro direct methanol fuel cell stack
Micro-electromechanical system
Anode flow fields
Polydimethylsiloxane

ABSTRACT

In this work, we present a 4-cell air-breathing micro direct methanol fuel cell (μDMFC) stack featured with novel n-inlet and n-outlet (NINO) anode flow fields. Compared with the conventional parallel flow field, the NINO flow field with micro structures improves the methanol solution transport efficiency and facilitates the exclusion of $CO_2$ gas bubbles accumulated in flow channels. The μDMFC stack patterned with novel NINO flow field is fabricated using silicon-based micro electromechanical system (MEMS) technologies. The polydimethylsiloxane (PDMS) distributors are used not only for the stack packaging but also for the uniform distribution of methanol solution through the connected double-side patterns. Experimental results reveal that the NINO flow fields exhibit higher peak power density than that of the conventional flow field. The NINO structures with different patterns have significant influences not only on the momentum transfer but also on the cell performance. The maximum power output of the μDMFC stack can yield about 80 mW at room temperature, which is significative for portable applications.



## 1. Introduction

In the past few years, the demand for the efficient and renewable energy sources is increasing rapidly with the functionalities of portable devices. As one type of polymer electrolyte membrane fuel cell (PEMFC), DMFC has been attracting more attentions due to its fast response to dynamic loads, high theoretical energy density and quick start-up [1–5]. With the development of MEMS technologies, μDMFC has obviously become the breakthrough point to the micro power sources in future due to their reduced size and easy to be integrated along with other micro-devices [6–8].

Basically, the DMFC includes two current collectors (anode and cathode) and a membrane electrode assembly (MEA) between them. The MEA is generally composed of two diffusion layers, two catalyst layers, and a proton exchange membrane (PEM). As illustrated in Fig. 1, in the μDMFC electrochemical process, the methanol diffuses from the anode flow field through the diffusion layer to the catalyst layer. The methanol solution is oxidized into protons, carbon dioxide and electrons. The protons are transferred to the cathode catalyst layer through the PEM, the electrons collected by the anode current collector are transported to the cathode via the external circuit, and the carbon dioxide accumulated is removed with the methanol flow. At the same time, oxygen is converted into water combined with protons and electrons. The overall oxidation–reduction process can be defined as:

$$2CH_3OH + 3O_2 \rightarrow 2CO_2 + 4H_2O \quad (1)$$

A practical power source is usually composed of a number of single cells, such combination is called fuel cell stack, which can provide high power to support electronic products [9]. Among several factors that have influences on μDMFC performance, the anode flow field should accomplish the following functions such as distributing reactants uniformly over the active areas, sustaining diffused layer, and providing the paths for the removal of reaction-generated gas $CO_2$ from the cell, especially in the cell stack [10]. The parameter optimizations and new configuration designs have identified a favorite topic by many industry observers. At present, there are mainly three kinds of materials being investigated for the current collector of the μDMFCs, including silicon, metal, and polymer [11]. Thanks to the MEMS technology, micro features fabricated on the silicon wafer can possess high repeatability. Zhou et al. presented a mathematical model to describe the conventional NINO flow field. The simulation results revealed that the NINO flow field made the distribution of pressure more general. Velocity and polarization curve was also investigated in this model [12]. Zhong et al. developed a silicon-based μDMFC stack, showing a power density of 12.71 mW $cm^{-2}$. Micro fabrication and PDMS assembly were used to implement the stack. The anode flow channels featured with single serpentine patterns were optimized by simulations [13]. Cao et al. fabricated two mono-polar 6-cell μDMFC stacks with two different anode flow fields on silicon substrates, and experimental results showed that the stack with double serpentine-type

* Corresponding author at: MEMS Center, Harbin Institute of Technology, Harbin 150001, China. Tel.: +86 451 86413451; fax: +86 451 86413441.
*E-mail address:* yufeng_zhang@hit.edu.cn (YF. Zhang).

0378-7753/$ – see front matter © 2011 Elsevier B.V. All rights reserved.
doi:10.1016/j.jpowsour.2011.10.090

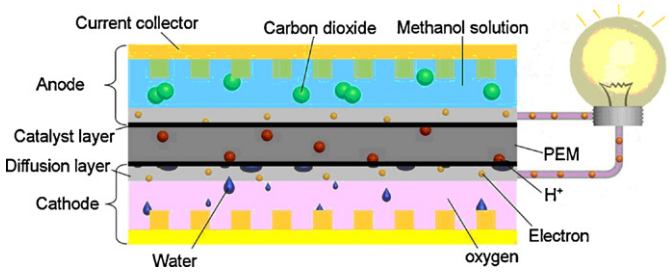


**Fig. 1.** Basic principle of a μDMFC.

flow fields could generate a better performance with the maximum output power reaching 151 mW at a voltage of 1.5 V [14].

In the literatures reported in the past few years, two conventional flow fields (parallel channel and single serpentine channel) are generally applied in the anode configurations. However, conventional parallel flow field results in the low fuel diffusion and mass transport owing to the low pressure and mean fuel velocity [12,15]. Based on these understandings, the objective of this work was to study a 4-cell air-breathing μDMFC stack with novel n-inlet and n-outlet (NINO) flow fields, which single channel possesses an input and an output. The structure can guaranteed the well-distributed methanol in every parallel channels with the unification of methanol concentration at the inputs, and the gas $CO_2$ can be removed immediately. The structure of this stack could reduce the volume effectively. A mathematical model was presented to describe the new flow field. The simulation results revealed that the NINO flow field with micro structures made the concentration more equal and enhanced the pressure difference with the same channel area of conventional parallel flow fields. The air-breathing single cell and μDMFC stack were designed and fabricated by silicon-based MEMS and PDMS technologies [16]. The flow field with different micro-features was experimentally investigated to prove the superiority of this novel flow field.

## 2. Simulation of the anode flow field

### 2.1. Model description and assumption

To better understand the influence of four types of NINO anode flow fields on the cell performance, a three-dimensional steady-state mathematical model was developed. In this model, more attention was paid to the influence on the transportation of reactants in anode active area, including anode flow channels, diffusion layer and catalyst layer. Several simplifications assumptions are introduced in this model: (1) all processes in the μDMFC are under steady-state conditions; (2) the difference of temperature inside the cell is neglected; (3) the methanol crossover through proton exchange membrane (PEM) is neglected.

### 2.2. Governing equations

The transport of methanol solution in the anode flow field and diffusion layer takes two transport mechanisms (convection and diffusion) into account. Therefore, in the model descriptions, the convection–diffusion equation is utilized to characterize the methanol mass distribution in the flow field and diffusion layer (Table 1):

$$\nabla \cdot (-D_i \nabla C_i + u_j C_i) = S_i \tag{2}$$

The diffusion coefficient of methanol in the diffusion layer can be expressed as:

$$D = D_{eff} \cdot (\varepsilon)^{1.5} \tag{3}$$

**Table 1**
Nomenclature used in equations of the μDMFC model.

| Nomenclature | |
|---|---|
| $C$ | Molar concentration (mol m$^{-3}$) |
| $D$ | Diffusivity (m$^2$ s$^{-1}$) |
| $F$ | Faraday's constant (C mol$^{-1}$) |
| $i$ | Current density (A m$^{-2}$) |
| $k_r$ | Relative permeability |
| $K$ | Permeability |
| $N$ | Molar flux (mol m$^{-2}$ s$^{-1}$) |
| $p$ | Pressure (Pa) |
| $R$ | Gas constant (mol m$^{-3}$ s$^{-1}$) |
| $H$ | Mass source term |
| $u$ | Velocity (m s$^{-1}$) |
| $V_{cell}$ | Cell voltage (V) |
| $S$ | Specific surface area (m$^{-1}$) |
| $E_{cell}$ | Thermodynamic equilibriumpotential (V) |
| *Greek alphabet* | |
| $\alpha$ | Charge transfer coefficient |
| $\delta$ | Conductivity (S m$^{-1}$) |
| $\phi$ | Cell potential (V) |
| $\rho$ | Density (kg m$^{-3}$) |
| $\mu$ | Dynamic viscosity (N s m$^{-2}$) |
| *Subscripts* | |
| $a$ | Anode |
| $c$ | Cathode |
| $i$ | Methanol |
| $j$ | Gas or liquid |
| $ref$ | Reference value |
| $eff$ | Effective value |
| $s$ | Electronic value |
| $l$ | Free electrolyte value |

The incompressible Navier–Stokes equations can be applied to describe the momentum transport in the flow field. The flow of methanol solution in anode channels is considered to be laminar flow.

$$(u_j \cdot \nabla)u_j = F - \frac{1}{\rho_j}\nabla p_j + \frac{\mu_j}{\rho_j}\nabla^2 u_j \tag{4}$$

$$\nabla \cdot u = 0 \tag{5}$$

Diffusion layer is modeled as porous media and volume average velocity of phase $j$ is calculated by continuous function based on Darcy's law:

$$\nabla \cdot \left(\rho_j \left(-\frac{Kk_{rj}}{\mu_j}\nabla p_j\right)\right) = H_j \tag{6}$$

$$u_j = -\frac{\kappa}{\eta}\nabla p_j \tag{7}$$

The transportations of electron and proton are respectively controlled by solid-phase electronic potential and membrane ionic potential. As the overlay region of solid and electrolyte, the catalyst layer enhances the overall reaction by providing the reaction channel for electrons, protons and related reaction molecules. Obviously, the electronic current flows in diffusion layer and catalyst layer, while the ionic current resides in catalyst layer and PEM [17]. There is no electrochemical reaction in the diffusion layer, so the source term of electronic current is set to be zero and expressed as follows:

$$-\nabla(-\sigma_s \nabla \phi_s) = 0 \tag{8}$$

Similarly, the source term for the ionic current in PEM should be zero.

$$-\nabla(-\sigma_l \nabla \phi_l) = 0 \tag{9}$$

where $\sigma_s$ is the electronic conductivity (S m$^{-1}$). $\phi_s$ is the over potential in catalyst layer (V). $\sigma_l$ represents conductivity of the free electrolyte (S m$^{-1}$) and $\phi_l$ is the electrolyte over potential (V).

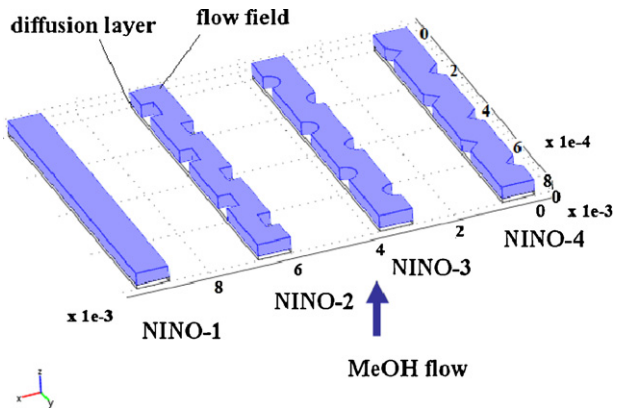


**Fig. 2.** Schematic of simulation domains of the three-dimensional model for the NINO anode flow field.

The catalyst layer is the region where reaction happens and the ionic balance and electron balance are described as follows:

$$-\nabla(-\sigma_{l,eff}\nabla\phi_l) = -S_a i_c \quad (10)$$

$$-\nabla(-\sigma_{s,eff}\nabla\phi_s) = S_a i_c \quad (11)$$

The anode current density generated by the methanol oxidation in the catalyst layer can be described by Tafel equation:

$$i_a = i_0 \cdot \exp\left(0.5F\frac{eta}{RT}\right) \cdot \left(\frac{c}{c_{ref}}\right) \cdot (c \geq 0) \quad (12)$$

The coupled equations were numerically solved by finite element method using COMSOL Multiphysics. Based on the three-dimensional model, we have investigated the impact of NINO anode flow field with micro-features. The model geometry is illustrated in Fig. 2. The figure shows the flow channel and diffusion layer of four structures respectively, with the width of micro flow channel of 0.8 mm, the length of 8 mm and the depth of 0.3 mm. The high of diffusion layer is 0.1 mm. The initial methanol concentration is 1.0 mol $L^{-1}$ and the flow rate of inlet is set of 0.0345 m $s^{-1}$.

### 2.3. Simulation results

Anode flow fields from NINO-1 to NINO-4 were investigated at the same reaction parameters and cathode structures. Fig. 3 demonstrates the superiority of the anode flow field with rectangle patterns (NINO-2). The simulation result of Fig. 3(a) indicated that the channel with micro features has a higher pressure difference than the smooth channel without features, and the flow pattern with rectangle patterns has the highest pressure difference. The pressure difference of channels decreased in the following sequence as NINO-2, NINO-3, NINO-4 and NINO-1, which were calculated of 69.43,55.34,34.36 and 10.53 Pa, respectively. This is due to the fact that the length of channel is longer than others and this channel could make the solution flow in a zigzag shape. The higher pressure could accelerate the velocity of anode reactants, as shown in Fig. 3(b). The higher liquid velocity enhances the mass transfer of methanol from the flow channel to the diffusion layer, improving the μDMFC performance. In addition, higher pressure and velocity facilitate the discharge of $CO_2$ gas bubbles accumulated in flow channel, causing the effective contact area between methanol solution and the gas diffusion layer to become larger. Simulated results indicate that micro-features have a significant influence on the mass transport of the μDMFC, and the NINO-2 flow field exhibits the best transport characteristic.

As seen from Fig. 3(c) and (d), the methanol concentration and current density on the surface of catalyst layer are higher than flow fields with semicircle, and triangle features. Based on calculations, the maximum methanol concentrations in the catalyst layer from NINO-1 to NINO-4 were 938.32, 943.52, 942.56 and 940.86 mol $m^{-3}$, and the highest current densities in the catalyst layer of four patterns were 2521.32, 2528.46, 2526.10 and 2523.58 A $m^{-2}$. The simulation results, overall, indicated that the cell equipped with NINO-2 could exhibit higher-efficiency mass transport than the other three flow fields, and could yield a higher power density as shown in Fig. 4, making this structure available for the anode of μDMFC stack.

## 3. Fabrication and assembly

In this paper, an air-breathing μDMFC stack with novel anode flow field was proposed. A schematic of the basic structure and key components of the 4-cell μDMFC stack which is connected in series is shown in Fig. 5. The stack is composed of two stack fixers, two end plates, two distributors, one anode monopolar plate, three one-side bipolar plates, one cathode monopolar plate, a MEA of four pairs of electrodes, and sealing gaskets. The electrical interconnection is achieved by Ti/Au layers sputtered on the one-side bipolar plates. Through the drilled ducts of the polycarbonate (PC) fixers and end plates, methanol solutions can be fed into the micro-channels of back sides of the PDMS distributors, and then distributed to each individual μDMFC at the front sides via the holes uniformly. Meanwhile, several windows were fabricated on the end plates and distributors to make cathode ventilated to air. Fig. 6(a) shows the design of the NINO flow field in the μDMFC anode plates, including the micro-features fabricated in the flow channels which are detailed as rectangle, semicircle, and triangle (represented by NINO-2–4). Parameters of the flow field patterned with rectangle tooth are shown in Fig. 6(b), the depth of corrosion is 300 μm. The gap of semicircle and triangle are identical with that of rectangle.

Take the simulation parameters into account from Figs. 2 and 6, both the anode and cathode current collectors with different structures and parameters were manufactured following a series of MEMS fabrication steps, as shown in Fig. 7. First, a 1 μm thick layer of $SiO_2/Si_3N_4$ for an etching mask was grown on a 500 ± 20 μm thick 3-in. polished silicon wafer substrate by the thermal oxide and LPCVD methods. To make micro flow fields, the mask layer was patterned by photolithography. Then, the $SiO_2/Si_3N_4$ mask layer was removed by RIE and HF solutions. Afterwards, the flow fields were etched using anisotropic etching process by KOH solutions with a concentration of 40% at 40 °C. To shape the feeding holes, another alkaline etching process by electrochemistry reaction was carried out to fabricate straight through-holes with the diameter of 600 μm. At last, in order to provide the current collectors with low contact resistance, an Au layer with the thickness of 2000 Å was sputtered onto the surface of the silicon wafer. Fig. 8 shows the picture of the Au-plated anode current collectors with the single cell active area of 1.0 cm × 1.0 cm, the air-breathing holes were perforated by laser beam.

The heart of a DMFC is a membrane electrode assembly (MEA) by sandwiching between an anode and a cathode. In this work, the MEA was fabricated by the catalyst coated membrane (CCM) method with an anode catalyst layer of Pt–Ru back (4.0 mg $cm^{-2}$) and a cathode catalyst layer of Pt back (2.0 mg $cm^{-2}$) and a Nafion117 membrane between them. First, the hydrophilic catalyst layers were prepared using the decal transfer method to form the CCM. Afterward, carbon paper (TGPH-090, Toray Inc.) was prepared with the hydrophobic (10 wt.% PTFE for anode and 30 wt.% PTFE for cathode) and pore-formed ($NH_4HCO_3$) pretreatment to form the diffusion layers. Finally, the 5-layered MEA was achieved with the

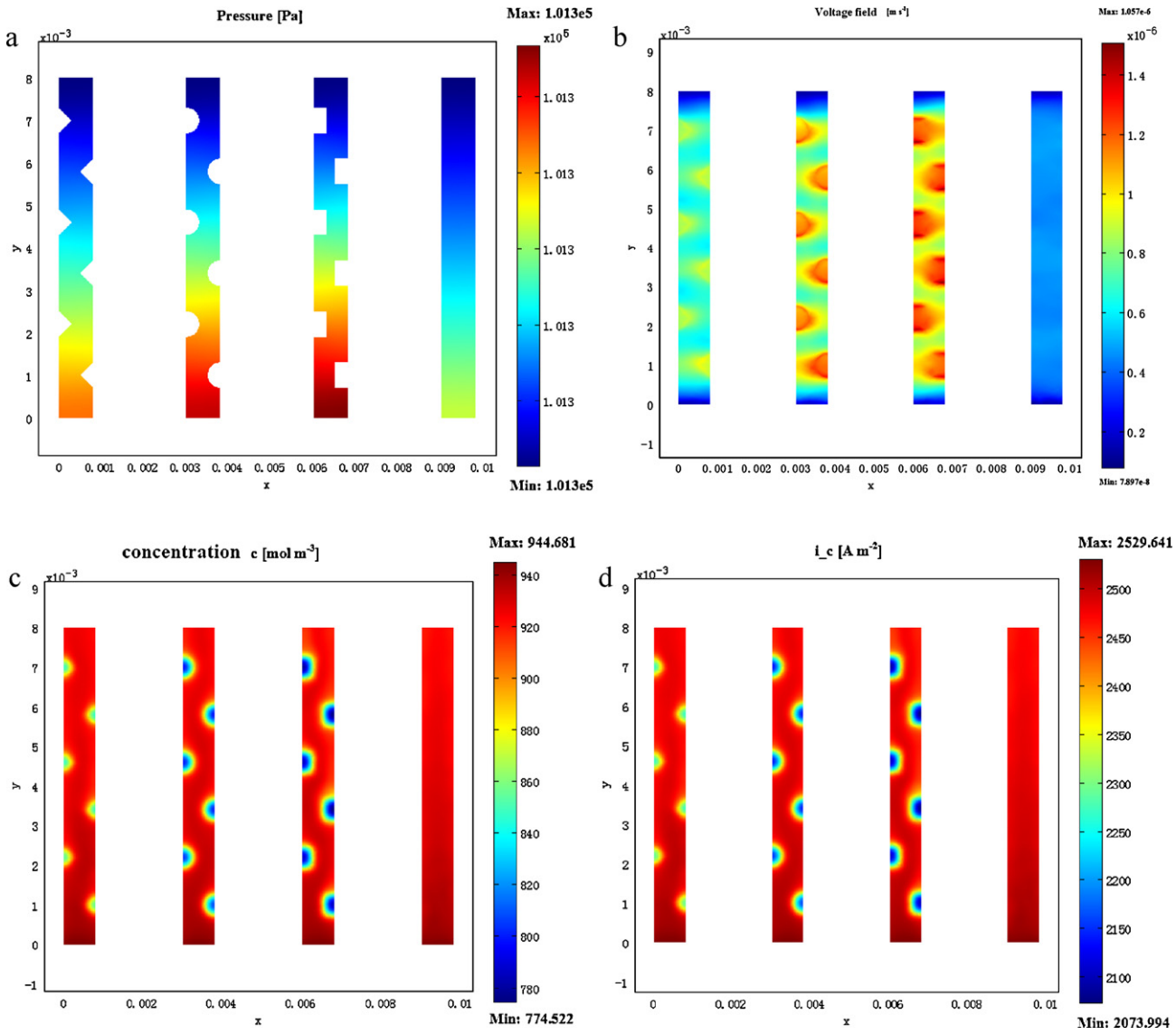


**Fig. 3.** (a) Pressure distribution on the surface of catalyst layer with different NINO structures. (b) Velocity distribution with different NINO anode structures. (c) Methanol concentration distributions at the catalyst layers with different NINO structures. (d) Current density distributions at the catalyst layers with different anode structures.

diffusion layers hot pressed on both sides of the CCM at 130 °C and 4 MPa for 120 s.

The double-side fabrication process of the PDMS distributor is described in Fig. 9. The size matched parameters of the current collector, which could effectively prevent the fuel leakage. Two 2 mm thick stainless steel plates were first milled and cleaned, and then micro machined with the patterns which were on both sides of the distribution plate. Afterwards, the stainless steel plates were hot embossed onto the surface of two 3 mm thick polymethyl methacrylate (PMMA) plates for 600 s, under the pressure of 2 MPa and at 90 °C. Then, a vacuumized 10:1 weight ratio PDMS elastomer and curing agent was poured between the face-to-face PMMA molds in a vacuum drying oven at 65 °C. After 1 h, the PDMS distributor with the double-side patterns was molded. At last, the holes and windows were achieved by the laser cutting technology.Finally, the whole device was obtained by mounting two silicon-based chips acting as current collectors together with PDMS encapsulation. Anode and cathode fixer plates with four unit cells were clamped by ten M3 screw joints. The photograph of the assembled stack is shown in Fig. 10. This structure could effectively avoid any fuel leakage or short circuit between the anode and cathode.

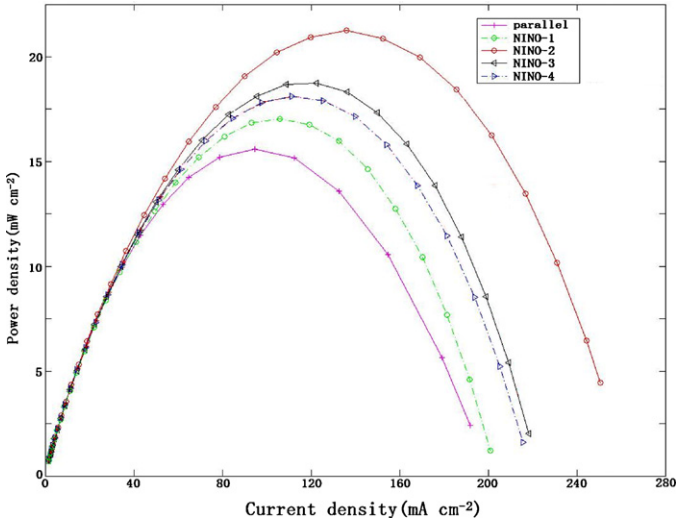


**Fig. 4.** Simulation results of the effect of anode flow field on the μDMFC performance.

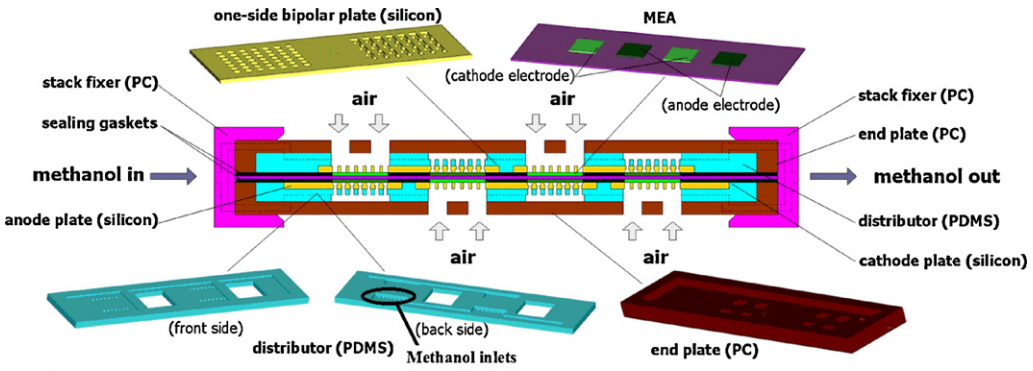


**Fig. 5.** Basic structure and key components of the 4-cell μDMFC stack design.

## 4. Results and discussion

Before the cell performance test, the MEA was required an activation process to achieve the optimal condition, the activation process via changing current was explored. Firstly, 90 °C deionized water was fed into the μDMFC anode flow field and 80 °C saturated oxygen to the cathode side at ambient pressure to humidify the MEA for 1 h. Secondly, to activate the catalysts, the cell maintained at 10 mA after making the open voltage stable, with 2.0 M methanol solution at 5.0 mA $min^{-1}$ to the anode and 85 °C saturated oxygen at

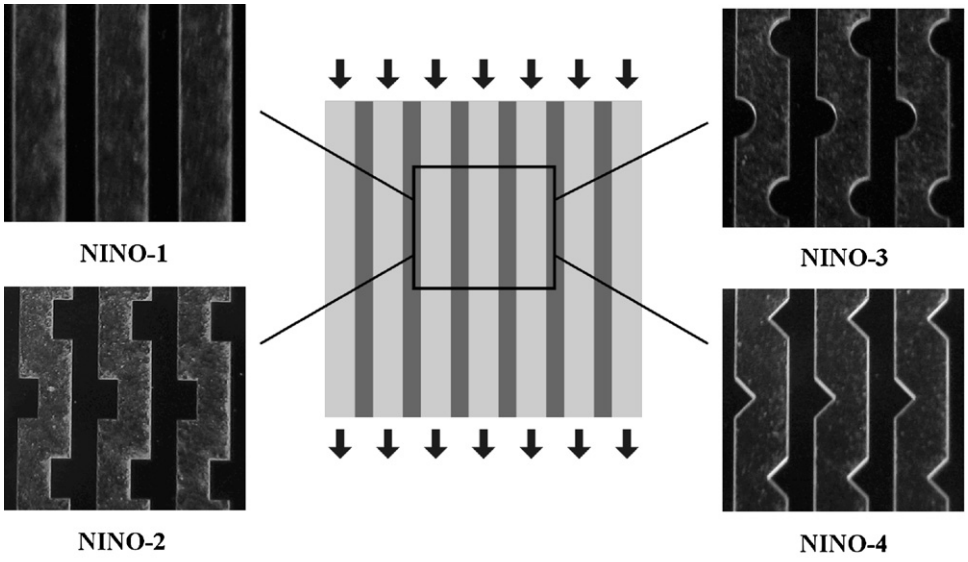


(a) The design of the NINO flow field in the μDMFC anode plates

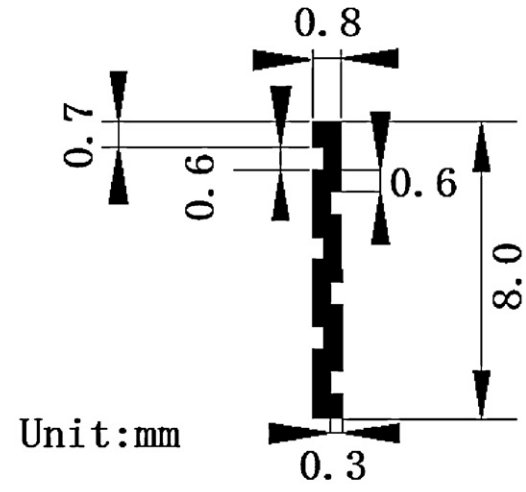


(b) Flow field parameters of NINO-2

**Fig. 6.** (a) The design of the NINO flow field in the μDMFC anode plates and (b) flow field parameters of NINO-2.

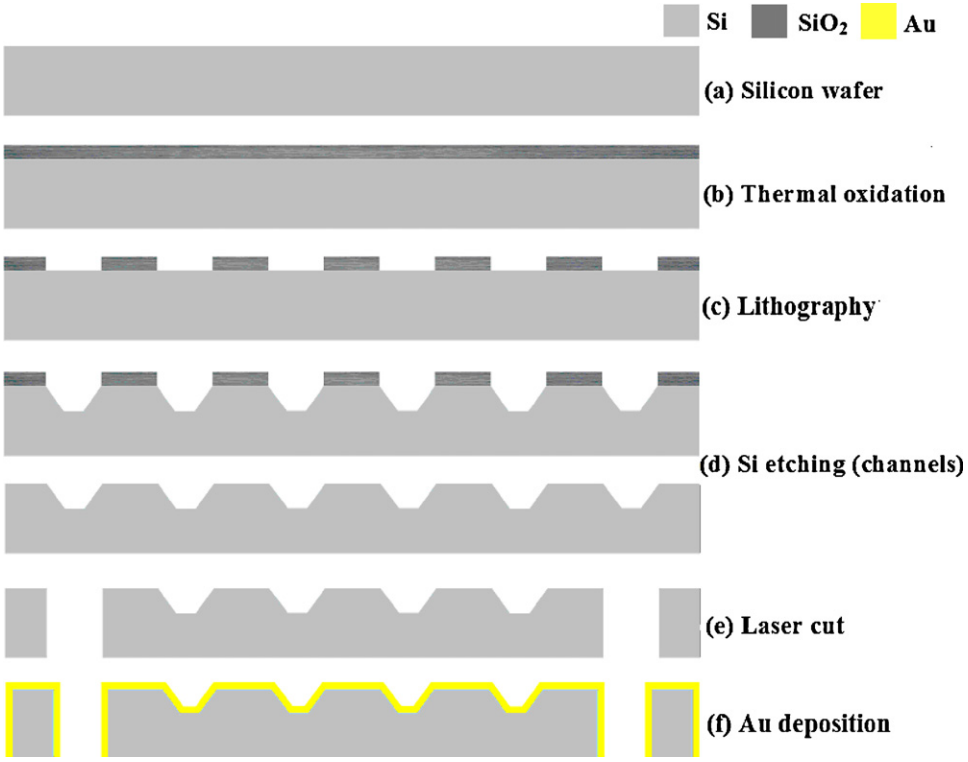


**Fig. 7.** Schematic of the fabrication process of the silicon-based current collector.

720 ml min$^{-1}$ and 25 psig to the cathode. Thirdly, the cell discharge current increased with 0.3 mA min$^{-1}$ until the limit current state and the whole activation process would keep 10 h. Under these conditions, the MEA could meet the experimental requirement.

### 4.1. Single cell performance

In order to obtain the reference data for a better understanding of the air-breathing μDMFC stack, a set of experiments was firstly carried out to investigate and optimize the single μDMFC performance at room temperature.

The effect of the anode flow rate (0.5, 1.0 and 2.0 ml min$^{-1}$) was investigated as shown in Fig. 11. The cell was operated with 1.0 M aqueous methanol solution at 20 °C. The decrease of open voltage from 0.5 to 2.0 ml min$^{-1}$ indicated that the rate of methanol crossover increased with the increase of flow rate. The output power density had an obvious improvement with the flow rate increased from 0.5 to 1.0 ml min$^{-1}$. The improved performance was attributed to the fact that the transport resistance caused by porous structure of diffusion layer and $CO_2$ gas bubbles could be weakened with the increase of flow rate, especially in micro-scaled channels. However, with the increase of the flow rate from 1.0 to 2.0 ml min$^{-1}$, the methanol crossover rate would be increased. Moreover, in this rate region, the higher pressure caused by higher flow rate would restrict the cathode mass transport.

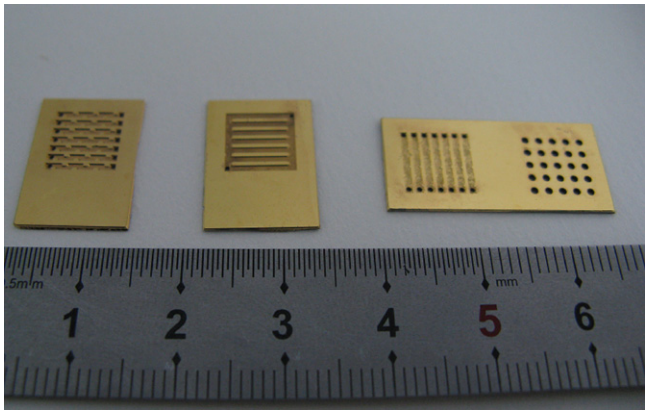


**Fig. 8.** Picture of the Au-plated anode current collectors with the single cell active area of 1.0 cm × 1.0 cm.

The performance of the air-breathing μDMFC operated with different methanol concentrations from 0.5 to 2.0 M is depicted in Fig. 12. The related experiments were carried out at the same anode flow rate of 1.0 ml min$^{-1}$ at 20 °C. It is seen that the open voltage decreased with the methanol concentration increased from 0.5 to 2.0 M, and the maximum open voltage of 552.2 mV was obtained when the cell filled with 0.5 M methanol solution. The phenomenon is due to the fact that the methanol crossover increased with the increase of concentration. The optimal performance was measured of 16.9 mW cm$^{-2}$ with the concentration of 1.0 mol L$^{-1}$. The higher methanol concentration could bring about a declination of the cell performance, especially at low current region. This behavior indicates that excess amounts of methanol left after the electrochemical reaction induces the methanol crossover and generates over-potential at the cathode. The lower performance at low methanol concentration can be associated with the fact that lower methanol concentration hardly provides sufficient reactants to join the electrochemical reaction, especially at high current densities. For example, the cell performance with the 0.5 M methanol solution declined sharply when the current density was more than about 80 mA cm$^{-2}$.

Fig. 13 exhibits the performance curves of the single cell between conventional parallel and NINO-2 flow fields, the related experiments were conducted with 1.0 M methanol solution fed at 1.0 ml min$^{-1}$. As seen from the figure, the cell performance was effectively improved with the maximum power density enhanced from 10.6 mW cm$^{-2}$ to 16.9 mW cm$^{-2}$ after improving the anode structure. We also found that the parallel-based DMFC performance

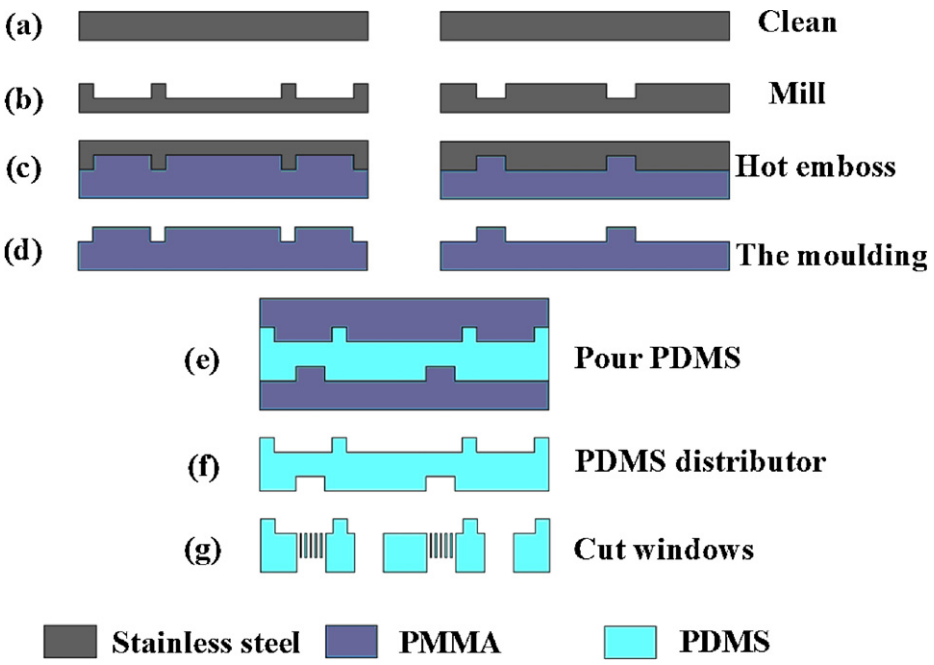


**Fig. 9.** The double-side fabrication process of the PDMS distributor.

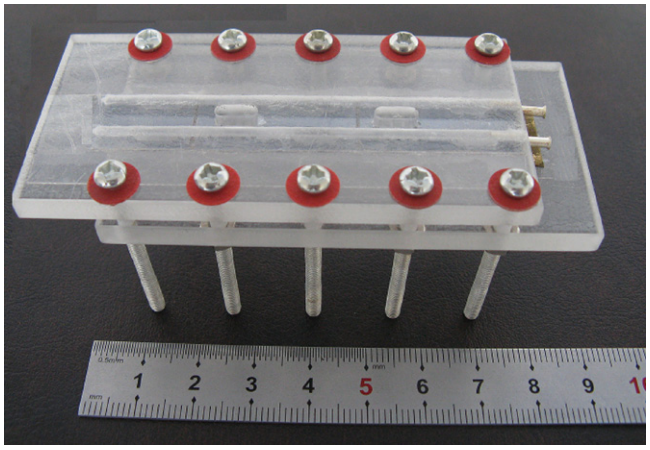

**Fig. 10.** The photograph of the assembled stack.

decreased sharply at the current density region of 90 mA cm$^{-2}$. The lower performance due to the fact that conventional parallel flow field will cause a uneven distribution of methanol solution in the diffusion layer because of its low pressure, weakening the methanol mass transfer and thereby causing degradation in the cell performance. The mass transport dead angle will also cause the phenomenon of concentration polarization. Moreover, the lower pressure of conventional parallel flow field decreases the fuel velocity, restricts the sweeping rate of $CO_2$ bubbles accumulated in channels, which will reduces the effective contact area. Consequently, the supply of liquid reactant through the gas diffusion layer to the catalyst layer will be restrained, it has a negative effect on the cell performance.

The mass-transport rate from the channel to the electrode is another indication to denote the methanol solution transport. The preceding analysis demonstrated that the mass transport rate of NINO-based anode could be significantly enhanced compared with

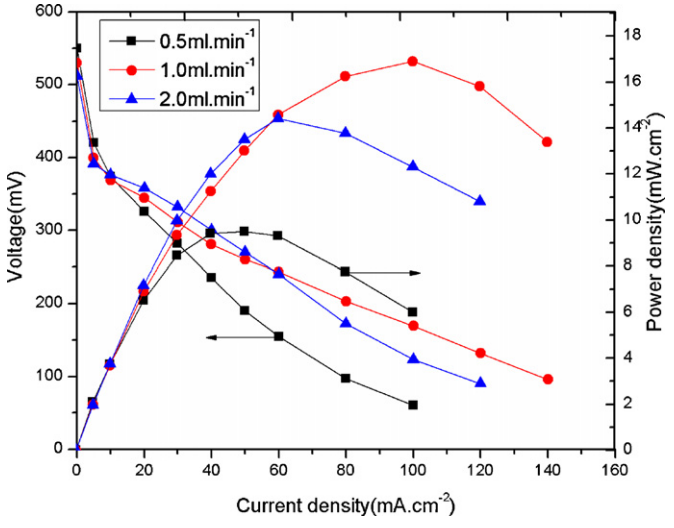


**Fig. 11.** Power density curves of the DMFC at different anode flow rates.

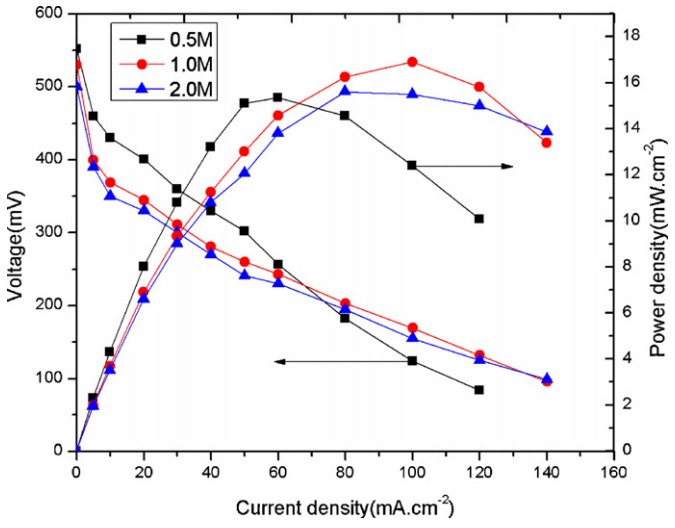


**Fig. 12.** Performance curves of the DMFC with different methanol concentrations.

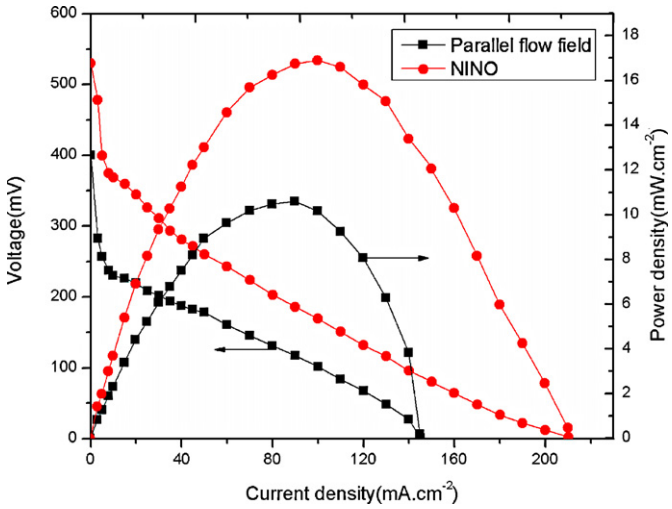


**Fig. 13.** The performance curves of the single cell between conventional parallel and NINO-2 flow fields.

the conventional parallel flow field. The overall mass transport coefficient from the channel to the electrode could be calculated by measuring the limiting current density [18]:

$$k_{tot} = \frac{i_{\lim}/6F}{C_0 - (i_{\lim}A/12Fu_0)} \tag{13}$$

where $C_0$ represents the methanol concentration at the channel inlet (1.0 M), $i_{\lim}$ is the limiting current density controlled by mass transport (145 mA cm$^{-2}$ for the parallel flow field and 210 mA cm$^{-2}$ for NINO one, as shown in Fig. 13), $F$ is the Faraday constant (96,495 C mol$^{-1}$), $u_0$ is the given inlet flow rate (1 ml min$^{-1}$), and $A$ is the area of the electrode region (1.0 cm$^2$). The corresponding mass transport coefficients were calculated using Eq. (13), achieving $2.50 \times 10^{-6}$ m s$^{-1}$ for the conventional parallel flow field and $3.63 \times 10^{-6}$ m s$^{-1}$ for the NINO one. An increase of 45.2% showed that methanol mass transport rates with the NINO flow fields were obviously improved, enhanced mass-transport rates from the channel to the electrode.

Fig. 14 illustrates the effect of four NINO micro-features on the performance of single μDMFC. The experiments were carried out at the air-breathing environment, with the same methanol concentration of 1.0 M at the flow rate of 1.0 ml min$^{-1}$. As illustrated in Fig. 14, the power density was almost equal at a low current level, but the difference increased with the increase of current density. The peak

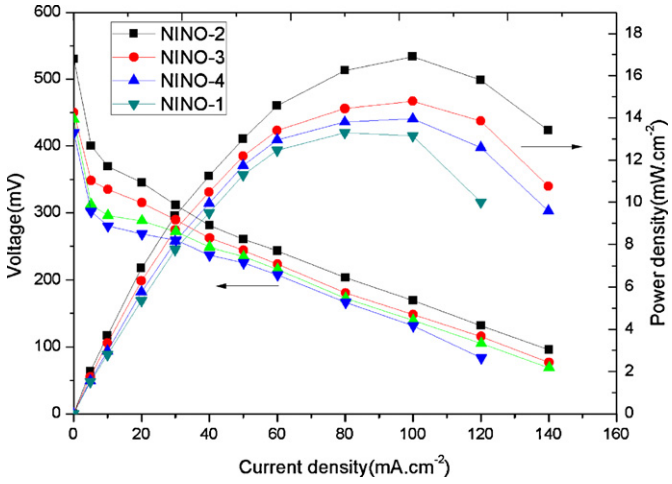


**Fig. 14.** The effect of four NINO micro-features on the performance of single μDMFC.

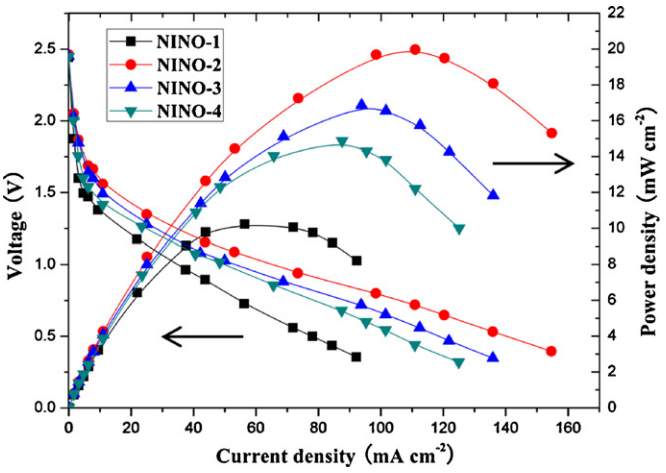


**Fig. 15.** The performance curves of the μDMFC stack.

power density was 13.3 mW cm$^{-2}$, 16.9 mW cm$^{-2}$, 14.8 mW cm$^{-2}$ and 13.95 mW cm$^{-2}$ from NINO-1 to NINO-4, respectively. The improved performance is primarily attributed to the fact that at the same flow rate, the pressure in the NINO-2 flow field is higher than the other flow fields. The higher pressure enhances methanol transport rate, accelerates the methanol solution mass transfer to the micro-porous structure. The results obtained by experiment have regularity in common with simulation, the cell with NINO-2 could give a better mass transport than other patterns, therefore improved performance of the cell.

On the other hand, the effective area is strongly affected by $CO_2$ gas bubbles, because the $CO_2$ produced can occupy the transport channel and disturbs the liquid flow, especially at high current density region. The relationship between the quantity of $CO_2$ bubbles and current density can be explained from the equation [19]:

$$Q_{CO_2} = \frac{AM_{CO_2}}{6F\rho_{CO_2}} I \tag{14}$$

where $Q_{CO_2}$ represents the volume of $CO_2$ and $A$ is the active MEA area.

According to the equation, the volume of $CO_2$ should be equal with the same experimental conditions. However, the $CO_2$ volume was measured by drainage method with 1.0 M methanol solution supplied at a flow rate of 1.0 ml min$^{-1}$ at the current of 60 mA. It is interesting to notice that the measured volumes from NINO-1 to NINO-4 were 3.06 ml, 5.34 ml, 4.35 ml and 3.94 ml after 5 min (0.612 ml min$^{-1}$, 1.068 ml min$^{-1}$, 0.87 ml min$^{-1}$ and 0.788 ml min$^{-1}$), respectively. Moreover, the gas ejected from NINO-2 usually in a small discrete shape, whereas several slug bubbles ejected from NINO-1 flow field. This is due to the fact that the rectangle-based NINO-2 possessed larger area of micro features than the other NINO flow field, forming zigzag channel. The angle located in the intersection between parallel channel and microstructure is sharper than other structures, these angles can cut the $CO_2$ string into a number of discrete tiny bubbles. These small bubbles can be easily removed with a high rate under a high methanol solution flow field. Thus, the contact area between the methanol solution and the porous layer could be much larger and the reaction liquid in the anode channels could be steadier, which both beneficial to enhance the cell output power.

### 4.2. Stack cell performance

The air-breathing μDMFC stack with four different anode flow fields were investigated at room temperature with the optimal experimental parameters. Fig. 15 depicts the power curves of

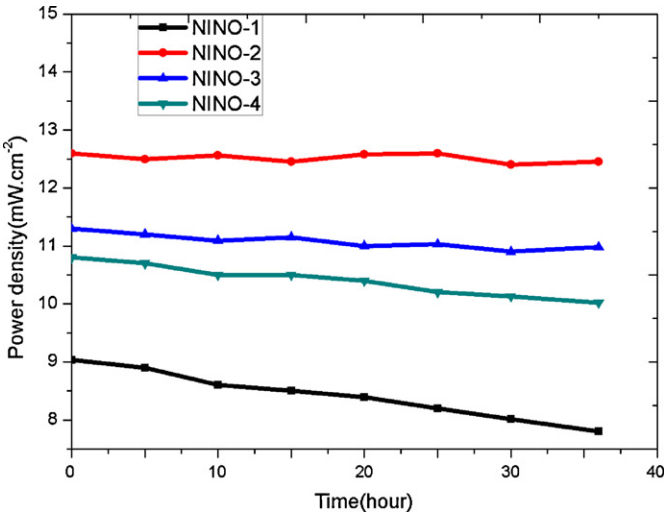


**Fig. 16.** Stack durability for the four anode patterns with the same operating condition.

the μDMFC stack. Obviously, the structure of anode channel had a crucial influence on the stack performance. The experimental results indicated that the NINO-2 flow field yielded better performance than those with other flow fields, and the maximum power output was generated about 79.88 mW (19.97 mW $cm^{-2}$), while NINO-4 led to the lowest power output which was approximately 40.80 mW (10.20 mW $cm^{-2}$). The reasonable explanations include two aspects. First, the higher liquid velocity enhances the mass transfer of methanol from the flow channel to the gas diffusion layer, thereby improving the cell performance. Secondly, $CO_2$ gas bubbles could easily occupy the anode flow field and disturb the liquid flow in the narrow channels, the anode flow with NINO-2 can decrease the size of bubble, and the effective contact area between liquid fuel and the gas diffusion layer to become larger. Moreover, the removal rate of smaller $CO_2$ gas bubbles would increase with a higher pressure and velocity.

Maintaining the current density at 35 mA $cm^{-2}$, Fig. 16 provides the stack durability for the four anode patterns with the same operating condition. Overall, the results indicate that the stack with NINO-2 and NINO-3 was relatively stable, while that of the stack with NINO-1 and NINO-4 gradually declined to various extents. Furthermore, the performance degradation was more serious for the stack with NINO-1. This behavior is mainly caused by the lower pressure in conventional NINO flow field than others, restrains the mass transport vertical to the flow channel. The lower pressure may also result in the fuel starvation of the single cell at the end of the stack. This phenomenon will lead to the cell reversal, which can bring about decline of the cell performance at the current density of 35 mA $cm^{-2}$. In fact, the cell reversal will make the irreversible breakage to the MEA, so it is necessary to avoid this phenomenon in the stack application.

## 5. Conclusion

4-cell air-breathing μDMFC stacks with NINO patterns have been developed in this paper. Bulk-silicon MEMS technology was introduced to fabricate anode and cathode current collectors on the 500 μm thick silicon wafer and a Au layer with the thickness of 2000 Å was deposited onto the surface. By adopting the distribution plates using PDMS, anode feeding patterns were achieved. Compared with conventional parallel channels, the improved NINO channel exhibited a roughly 60% enhancement on the power density. The influence of the NINO pattern on momentum transport and performance were also investigated by three-dimensional simulation and experimental methods, the best performance could yield 16.9 mW $cm^{-2}$. The stack performances with four NINO patterns were also studied. Experiment results reveal that the stack with NINO-2 can generate the best performance of 80 mW under the same operating conditions. Finally, air-breathing μDMFC stacks were applied to investigate the durability for 1 h, respectively, demonstrating its feasibility in portable applications.

## Acknowledgements

The work described in this paper was supported by the National Natural Science Funds of China (Nos. 60806037, 61076105 and 61176109), a grant from the Ph.D. Programs Foundation of the Ministry of Education of China (No. 20102302110026), the Natural Scientific Research Innovation Foundation in Harbin Institute of Technology (HIT. NSRIF. 2009008) and National Key Laboratory of Fundamental Science of Micro/Nano-Device and System Technology, Chongqing University (2009MS03).

## References

[1] S.K. Kamarudin, F. Achmad, W.R.W. Daud, Int. J. Hydrogen Energy 34 (2009) 6902.
[2] Y.H. Lu, R.G. Reddy, Int. J. Hydrogen Energy 36 (2011) 822.
[3] A. Kundu, J. Power Sources 170 (2007) 67.
[4] H. Yang, T.S. Zhao, Electrochim. Acta 50 (2005) 3243.
[5] A. Kamitani, S. Morishita, H. Kotaki, S. Arscott, J. Micromech. Microeng. 18 (2008) 125019.
[6] A. Kamitani, S. Morishita, H. Kotaki, S. Arscott, J. Power Sources 187 (2009) 148.
[7] Z.G. Shao, F.Y. Zhu, W.F. Lin, P.A. Christensen, H.M. Zhang, J. Power Sources 161 (2006) 813.
[8] S.K. Kamarudin, W.R.W. Daud, S.L. Ho, U.A. Hasran, J. Power Sources 163 (2007) 743.
[9] R.Z. Jiang, R. Charles, C. Deryn, J. Power Sources 126 (2004) 119.
[10] N. Torres, J. Santander, J.P. Esquivel, N. Sabaté, E. Figueras, P. Ivanov, L. Fonseca, I. Gràcia, C. Cané, Sens. Actuators B 132 (2008) 540.
[11] T. Pichonat, B. Gauthier-Manuel, Microsyst. Technol. 13 (2007) 1671.
[12] X.C. Zhou, W.Z. Ouyang, C.P. Liu, T.H. Lu, W. Xing, L.J. An, J. Power Sources 158 (2006) 1209.
[13] L.Y. Zhong, X.H. Wang, Y.Q. Jiang, Q. Zhang, Sens. Actuators A 143 (2008) 70.
[14] J.Y. Cao, Z.Q. Zou, Q.H. Huang, T. Yuan, L.Z. Li, B.J. Xia, H. Yang, J. Power Sources 185 (2008) 433.
[15] X.G. Li, I. Sabir, Int. J. Hydrogen Energy 30 (2005) 359.
[16] X.H. Wang, Y.A. Zhou, Q. Zhang, Y.M. Zhu, L.T. Liu, J. Micromech. Microeng. 19 (2009) 094012.
[17] J.J. Hwang, S.D. Wu, L.K. Lai, C.K. Chen, D.Y. Lai, J. Power Sources 161 (2006) 240.
[18] C. Xu, T.S. Zhao, Electrochem. Commun. 9 (2007) 497.
[19] H. Yang, T.S. Zhao, Q. Ye, J. Power Sources 139 (2005) 79.